Tellus (2005), 57B, 412–422
Printed in Singapore. All rights reserved

TELLUS

Long-term lidar observations of polar stratospheric clouds at Esrange in northern Sweden

By U. BLUM[1]*†, K. H. FRICKE[1], K. P. MÜLLER[1]‡, J. SIEBERT[1]§ and G. BAUMGARTEN[2],
[1]*Physikalisches Institut der Universität Bonn, D-53115 Bonn, Germany;* [2]*Leibniz-Institut für Atmosphärenphysik e.V., D-18225 Kühlungsborn, Germany*

(Manuscript received 15 November 2004; in final form 30 May 2005)

ABSTRACT

Polar stratospheric clouds (PSCs) play a key role in the depletion of polar ozone. The type of cloud and the length of time for which it exists are crucial for the amount of chlorine activation during the polar night. The Bonn University backscatter lidar at Esrange in northern Sweden (68°N, 21°E) is well equipped for long-term observation and classification of these clouds. Nearly continuous measurements through several winters are rare, in particular in wave-active regions like Esrange. Lidar measurements have been performed each winter since 1997—a total of more than 2000 h of observation time has been accumulated, including more than 300 h with PSCs. Analysis of this unique data set leads to a classification scheme with four different scattering characteristics which can be associated with four different cloud types: (1) supercooled ternary solution (STS), (2) nitric acid trihydrate (NAT), (3) ice and (4) mixtures of solid and liquid particles. The analysis of observations over seven winters gives an overview of the frequency of appearance of the individual PSC types. Most of the clouds contain layers of different PSC types. The analysis of these layers shows STS and mixed clouds to occur most frequently, with more than 39% and 37% of all PSC observations, respectively, whereas NAT (15%) and ice clouds (9%) are seen only rarely. The lidar is located close to the Scandinavian mountain ridge, which is a major source of orographically induced gravity waves that can rapidly cool the atmosphere below cloud formation temperatures. Comparing the individual existence temperature of the observed cloud type with the synoptic-scale temperature provided by the European Centre for Medium-range Weather Forecasts (ECMWF) gives information on the frequency of synoptically and wave-induced PSCs. Further, the analysis of ECMWF temperature and wind data gives an estimate of the transparency of the atmosphere to stationary gravity waves. During more than 80% of all PSC observations in synoptic-scale temperatures which were too warm the atmosphere was transparent for stationary gravity waves. Our measurements show that dynamically induced cooling is crucial for the existence of PSCs above Esrange. In particular ice PSCs are observed only in situations where there are gravity waves.

1. Introduction

Polar stratospheric clouds (PSCs) play a key role in the destruction of polar ozone (cf. Crutzen and Arnold, 1986). Heterogeneous chemical reactions on the surfaces of the cloud particles lead to activation of, for example, chlorine components (Peter, 1997), which in turn leads to the ozone hole in the polar spring (Solomon, 1999). There are different types of PSCs (McCormick et al., 1982; Pool and McCormick, 1988). PSCs of type I consist of HNO_3 and H_2O, either nitric acid trihydrate (NAT, type Ia) or H_2SO_4, HNO_3 and H_2O (supercooled ternary solution, STS, type Ib) (Toon et al., 1986). Type II PSCs comprise pure water ice (Steel et al., 1983; Browell et al., 1990). In addition to these classical PSC types several other types of PSC which contain the same constituents but have different mechanisms of formation, and thus slightly different scattering characteristics, have been described in the literature: for example, type Ic (Tabazadeh and Toon, 1996), type Ia enhanced (Tsias et al., 1999), type Id (Stein et al., 1999) or NAT rocks (Fahey et al., 2001; Carslaw et al., 2002). Lidars as well as other ground-based (Toon and Tolbert, 1995), airborne (Voigt et al., 2000) and spaceborne instruments (Spang et al., 2001; Höpfner et al., 2005) or a combination of different methods (Deshler et al., 2003) can determine the type of PSC independent of meteorological assumptions or microphysical modelling. Depending on the type of PSC, different temperatures of formation and existence have to be attained (MacKenzie, 1995). In the northern winter synoptic temperatures do not always fall below these temperatures, but waves in the atmosphere

*Corresponding author.
e-mail: ubl@ffi.no
†Present address: Forsvarets Forskningsinstitutt, N-2027 Kjeller, Norway.
‡Present address: Heinrich-Hertz-Berufskolleg, D-53117 Bonn, Germany.
§Present address: Allianz Versicherungs-AG, D-80802 München, Germany.

can lead to additional cooling of 10 K or more, which allows PSCs to form (Carslaw et al., 1998b). Atmospheric waves can be excited orographically, and in particular form in the lee of the Scandinavian mountains (Størmer, 1929; Volkert and Intes, 1992; Dörnbrack et al., 2002; Blum et al., 2004).

Recently Toon et al. (2000) reanalysed PSC observations from seven DC-8 flights during the 1989 Airborne Arctic Stratosphere Experiment (AASE) to find statistical results on the frequency of occurrence of different types of PSC, in particular of mixed clouds, as well as on the influence of lee waves on PSCs. In several other case studies the influence of the Scandinavian mountains on PSCs was also analysed; however, there has been no study involving a long-term observational data set and its analysis. Although there are several, long-term satellite observations (e.g. Pool and Pitts, 1994; Fromm et al., 2003, and references therein), the temporal and spatial resolution of these measurements—depending on the satellite's observation geometry—are too low to observe all synoptic-scale and all small-scale lee-wave induced PSCs. Thus long-term observations at fixed places of particular interest (e.g. in wave-active regions) with high temporal and vertical resolution are necessary to complement the comprehensive data set with global coverage of the satellite measurements.

Since January 1997 Bonn University has operated a Rayleigh/Mie/Raman backscatter lidar at Esrange (68°N, 21°E), near the Swedish city of Kiruna, about 150 km north of the Arctic circle (Blum and Fricke, 2005). This lidar is well equipped to observe clouds in the stratosphere. In this article we will present a comprehensive data set for PSCs at a wave-active location, classify these cloud observations, perform a statistical analysis on the rate of occurrence of the different cloud types and verify whether the observed clouds can exist at the synoptic-scale atmospheric temperatures represented by the T106 analysis of the European Centre for Medium-range Weather Forecasts (ECMWF) or whether additional cooling by atmospheric gravity waves is necessary to reach the existence temperature for the particular cloud type.

First we will describe the instrument, the method of analysis used to characterize the observed clouds and the method used to determine the transparency of the atmosphere to stationary gravity waves. Next the collected data set is presented. In Section 4 a classification scheme is developed and used to describe these clouds. Knowledge about the individual cloud types at each altitude enables us to compare the synoptic-scale temperature with the existence temperature. In Section 5 the conditions of occurrence of the observed PSCs are analysed. Finally the results are summarized.

2. Instrumentation and method of analysis

The Bonn University lidar emits short, linearly polarized light pulses of length 10 ns, repetition rate 20 Hz and wavelength 532 nm and collects the backscattered light with three Newtonian telescopes, each of diameter 50 cm. The backscattered light is analysed according to wavelength and polarization, detected by photomultipliers and registered by counting electronics. The time elapsed between the emission of a light pulse and the detection of the echo determines the scattering altitude. In our case the range gates are set to 1 μs, resulting in an electronic altitude resolution of 150 m. The Rayleigh scattered light at 532 nm wavelength is detected in two orthogonal polarization directions; light with the same plane of polarization as the emitted beam is called parallel polarized ($\parallel$) and light with the polarization plane perpendicular to that of the emitted beam is called cross-polarized ($\perp$) light. The lidar detects the sum of the backscatter signal from the molecules and the aerosols. The relative magnitude of the aerosol signal in the parallel and perpendicular polarization directions is determined by the depolarization ratio δ_{Aer} of the aerosols. Combined with the molecular depolarization this leads to different sensitivities for the detection of solid aerosol particles in parallel and perpendicular polarization. In addition to the backscattered light, the signal from the vibrational-Raman scattered light on molecular nitrogen at 608 nm wavelength is detected. This Raman signal serves as a signal of the molecular density of the atmosphere. These three intensities $I^{\parallel}_{532}$, $I^{\perp}_{532}$ and I_{608} are used to calculate physically meaningful quantities like the backscatter ratio R and the aerosol depolarization δ_{Aer}:

$$R_{\parallel}(z) \propto \frac{I^{\parallel}_{532}(z)}{I_{608}(z)}, \tag{1}$$

$$R_{\perp}(z) \propto \frac{I^{\perp}_{532}(z)}{I_{608}(z)}, \tag{2}$$

$$\delta_{\mathrm{Aer}}(z) = \frac{R_{\perp}(z) - 1}{R_{\parallel}(z) - 1}\,\delta_{\mathrm{Mol}}. \tag{3}$$

To calculate absolute values for the backscatter ratios, the Raman signal is normalized to the Rayleigh signal in the aerosol-free part of the atmosphere. In eq. (3) δ_{Mol} is the molecular depolarization. The measured value of δ_{Mol} depends on the width of the instrumental filter band path. For our data set the band path is given by an interference filter with a full width at half maximum (FWHM) of <3 Å. This excludes the rotational Raman band and thus results in the molecular depolarization of $\delta_{\mathrm{Mol}} = 0.36\%$ (Young, 1980). Depending on the PSC type the depolarization ratio can increase to several 10%. Due to the small molecular signal in the cross-polarized channel in comparison with the parallel polarized channel it can happen that for a weak PSC the aerosol signal in the parallel channel is overwhelmed by the molecular signal in the parallel channel while this does not happen in the perpendicular channel.

After the first winter campaign in January–March 1997 the optical configuration of the lidar was improved. A Brewster plate was inserted in the transmitter branch to clean up a residual depolarization of the transmitter. Thus the polarization of the emitted

light was different in January–March 1997 from that in later winters. If the emitted light is not perfectly linearly polarized or the geometrical alignment of the transmitter and the receiver is not perfect, the instrument detects an apparent aerosol depolarization $\delta_{\mathrm{Aer}}^{\mathrm{obs}}$ even if there are no depolarizing scatterers in the atmosphere (Biele et al., 2000). An imperfect system leads to an error in the depolarization which we determined by the observation of spherical and thus non-depolarizing particles. To identify spherical particles we analysed the PSC observations with only very low measured depolarization values $\delta_{\mathrm{Aer}}^{\mathrm{obs}} < \delta_{\mathrm{Mol}}$. For this purpose we used all data with $R_{\perp}^{\mathrm{obs}} < R_{||}^{\mathrm{obs}}$, which is a necessary and sufficient condition for $0 \leq \delta_{\mathrm{Aer}}^{\mathrm{obs}} < \delta_{\mathrm{Mol}}$. However, there is no possibility of selecting only non-depolarizing PSCs. All PSC observations with $R_{\perp}^{\mathrm{obs}} < R_{||}^{\mathrm{obs}}$ in the period 1998–2003 were checked. The mean aerosol depolarization of these data has to be between 0 and 0.35% and was assumed to be $\delta_{\mathrm{Aer}} = 0.15\%$. This value is consistent with the lidar data if the depolarization caused by the instrument δ_{l} is lower than 0.10%, as model calculations show. While the instrumental depolarization was $\delta_{\mathrm{l}} = 0.5\%$ in 1997, the analysis of the later data resulted in a mean instrumental depolarization of $\delta_{\mathrm{l}} = (0.00 \pm 0.01)\%$. Thus we only need a depolarization correction for the data from the first campaign. This correction primarily affects the backscatter ratio in the cross-polarization $R_{\perp}$ as well as the aerosol depolarization δ_{Aer}:

$$R_{\perp} = R_{\perp}^{\mathrm{obs}} + \left(R_{\perp}^{\mathrm{obs}} - R_{\parallel}^{\mathrm{obs}}\right) \delta_{\mathrm{l}}/\delta_{\mathrm{Mol}},$$

$$\delta_{\mathrm{Aer}} = \delta_{\mathrm{Aer}}^{\mathrm{obs}} - \frac{R_{\parallel}^{\mathrm{obs}} - R_{\perp}^{\mathrm{obs}}}{R_{\parallel}^{\mathrm{obs}} - 1}\,\delta_{\mathrm{l}}.$$

A detailed description of the analysis is given by Blum (2003).

To determine whether the observed PSCs are caused by synoptically cold temperatures we compared the existence temperatures of the individual cloud types with the ECMWF T106 temperature analyses, which of course do not show small-scale variations in the temperature field due to the temporal resolution of 6 h and the vertical resolution of 2–3 km in the middle stratosphere. However, this resolution is sufficient to describe the synoptic temperature field of the polar stratosphere. The existence temperatures for NAT are taken from Hanson and Mauersberger (1988) and the HNO_3 concentrations are taken from Gille et al. (1996). The STS formation temperatures are assumed to be 3 K below the NAT temperatures and the water ice frost-point temperatures are taken from Murray (1967) using a water vapour mixing ratio of 4.6 ppmv. Existence temperatures of mixed clouds are assumed to be the same as those of STS clouds. The calculated existence temperatures are quite stable against a change in the HNO_3 and H_2O concentrations. To change the existence temperature by 10 K the concentration has to change by one order of magnitude (Hanson and Mauersberger, 1988).

Orographically induced gravity waves can propagate from the Earth's surface to the stratopause or even higher when appropriate atmospheric propagation conditions exist. The transparency of the atmosphere for these waves can be estimated from the wind and temperature fields of the ECMWF analyses. Using the dispersion relation for medium-frequency waves ($N \gg \hat{\omega} \gg f$, where $N \approx 2 \times 10^{-2}$ Hz is the Brunt–Väisälä frequency, $\hat{\omega}$ the intrinsic frequency of the waves and $f \approx 3 \times 10^{-5}$ Hz the inertial frequency or Coriolis parameter), the vertical wavenumber is given by

$$k_z(z) = \frac{2\pi}{\lambda(z)_{\max}} = \frac{N(z)}{|\overline{u(z)_{\mathrm{h}}} - c_{\mathrm{ph}}|} \tag{4}$$

(e.g. Fritts, 1984), where $\overline{u(z)_{\mathrm{h}}}$ is the mean horizontal wind in the direction of wave propagation and $c_{\mathrm{ph}}(z)$ the horizontal phase speed of the wave. For stationary waves the horizontal phase speed relative to the ground is $c_{\mathrm{ph}} = 0\ \mathrm{m\ s^{-1}}$. Thus the maximum vertical wavelength $\lambda_{\max}(z)$ can be written as

$$\lambda_{\max}(z) = \overline{|u(z)_{\mathrm{h}}|} P(z)_{\mathrm{B}} \tag{5}$$

where $P(z)_{\mathrm{B}} = 2\pi/N(z)$ is the Brunt–Väisälä period. Critical levels imply that $\lambda(z)_{\max}$ approaches zero, which inhibits wave propagation. This theoretical case will never be achieved in reality, thus we assume the atmosphere to be transparent whenever $\lambda_{\max} > 1$ km. To excite orographically induced gravity waves, the boundary layer wind has to exceed a certain wind speed with an appropriate direction. The model analyses by Dörnbrack and Leutbecher (2001) suggest a wind speed of more than 10 m s^{-1} coming from west-northwest (300° ± 30°). These values correspond to inertial gravity waves excited on the Scandinavian mountain ridge with horizontal wavelengths of 100–1000 km which can be resolved by the mesoscale model MM5. As well as these waves, locally excited buoyancy waves with horizontal wavelengths between 3 and 30 km are seen in the lidar data and lead to PSC formation. The local hills around Esrange are not oriented in a southwest/northeast direction like the Scandinavian mountain ridge, thus the direction of the boundary layer wind is less important in this case. The direction of the boundary layer wind determines the direction of propagation of the excited gravity wave, which stays constant with altitude. Changing wind direction with altitude influences the possibility of vertical gravity wave propagation, as can be seen in the vertical wavelength which can propagate through the atmosphere (eq. 5).

3. Data Set

The Bonn University lidar was set up at Esrange in December 1996 and the first measurements were performed in January 1997. Up to winter 2003–2004 10 major measurement campaigns of more than 4 weeks' duration had been carried out during winter. Additionally there were a few measurements in November–December 1999 performed by the Institutet för Rymdfysik (IRF) Kiruna and some measurements during December 2000. Figure 1 shows the measurement times and the times with PSC observations. The interannual variability of

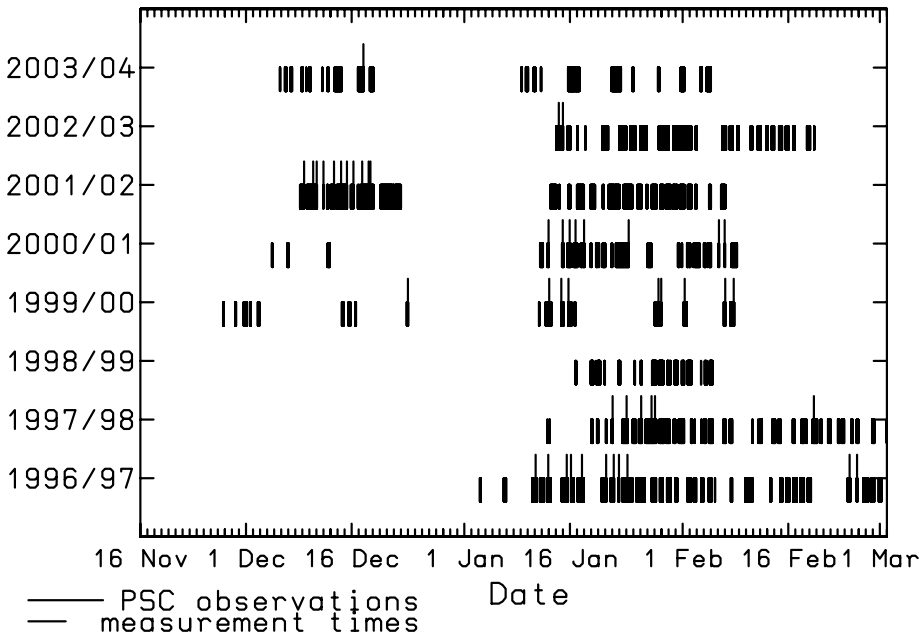

Fig 1. Distribution of measurement times of the Bonn University lidar during the winter campaigns 1996–1997 to 2003–2004. PSC observations during the measurement times are marked by longer lines.

PSC observations is quite large due to varying meteorological background conditions and changing campaign times.

During almost every winter campaign at least a few PSCs were observed with the Bonn University lidar. Whereas 26.5% and 11.1% of all PSC observations occurred during the winters of 1996–1997 and 1997–1998, respectively, the campaign in January and February 1999 was an exception, with no PSCs being observed. Due to a major stratospheric warming which developed during December 1998 (Labitzke and Naujokat, 2000) the stratospheric circulation including the polar vortex was disturbed and the stratospheric air did not cool down to the temperatures necessary for PSC formation. The following two winters 1999–2000 and 2000–2001 showed 5.8% and 15.6% of all PSC observations. Although winter 2001–2002 showed 38.6% of all PSC observations, these clouds only appeared in December 2001. During the last four campaigns (January–February 2002, January–February 2003, December 2003 and January–February 2004) there were almost no PSC observations at Esrange (0%, 2.3%, 0.2%, 0%). This absence of PSCs is again attributed to major stratospheric warmings which occurred during December 2001 (Naujokat et al., 2002), January 2003 (Naujokat and Grunow, 2003) and January 2004 (Labitzke et al., 2005). Altogether we accumulated more than 300 h of PSC observations during more than 2000 h of lidar measurements performed during these winter campaigns. Most of the PSC measurements at 532 nm wavelength in both polarization directions were carried out at night.

The PSC observations at Esrange are characterized by high vertical and temporal variability of the clouds which makes it extremely difficult to determine the temporal and spatial extension of each individual cloud. Figure 2 shows PSC data from 13 December 2001 in both polarizations for the three consecutive hours 18:00–19:00, 19:00–20:00 and 20:00–21:00 UT. The parallel polarization channel shows two distinct clouds delimited by regions of $R = 1$. The lower cloud reaches from 18.5–20.5 km during the first hour of observations and from 18.5–21.0 km later on. The upper cloud reaches from 23.0–25.0 km altitude through all 3 h. The perpendicular channel also shows several distinct regions containing PSC signatures. However, the vertical extent of these layers in this channel is very different from that in the parallel channel. The lower edge of the lower cloud and the upper edge of the upper cloud layer agree in both polarization channels. In contrast the region from 21–23 km altitude, which does not show any aerosol signal in the parallel channel, apparently contains values of $R_\perp > 1$. This cloud signature varies with time and indicates a rather weak PSC consisting of depolarizing (i.e. solid) particles. In addition to the large vertical variations which indicate different PSC types at different altitudes, there are also variations in the cloud characteristics with time. At about 23.7 km altitude the backscatter ratio increases and decreases during the 3 h of observations from $R_{||} \approx 4$ to $R_{||} \approx 16$ back to $R_{||} \approx 2$ in the parallel channel and from $R_\perp \approx 30$ to $R_\perp \approx 400$ back to $R_\perp \approx 60$ in the cross-polarized channel. This strong change in the backscatter ratio is caused by changes in the PSC type occurring during the observation time at this altitude. To cope with this high vertical and temporal variability of the clouds we treat each 150 m altitude interval—which is given by the vertical resolution of the lidar—as an individual PSC. The chosen temporal resolution

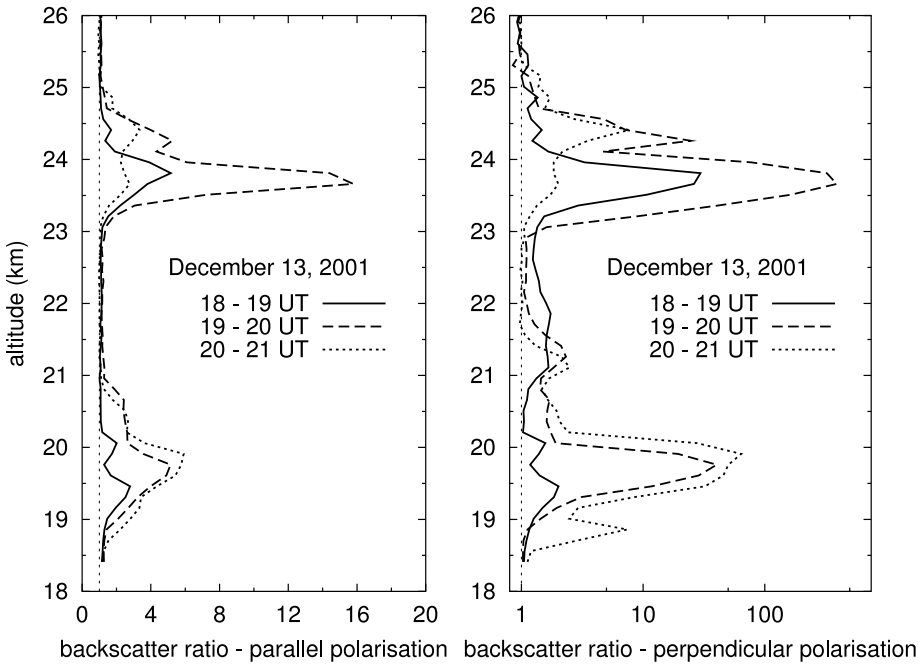

Fig 2. PSC measurements of the Bonn University lidar on 13 December 2001. Shown are the backscatter ratio profiles in parallel (left plot) and perpendicular (right plot) polarization for three consecutive hours.

must be short enough to resolve rapid changes in the PSCs but also long enough to achieve adequate data quality. An integration time of about 1 h using the UT time grid is a compromise for both requirements. This method of counting PSCs results in a large number of individual PSC observations; however, it is applicable for synoptic as well as wave-induced PSCs as we have not observed any correlation of the temporal and vertical extent of PSCs with the existence or absence of gravity waves.

4. Classification of PSCs

In lidar data PSCs are classified according to scattering parameters using the backscatter ratios $R_{||}$ and $R_{\perp}$, and the aerosol depolarization δ_{Aer}.

Although several classification schemes for lidar measurements of PSCs are available in the literature (e.g. Browell et al., 1990; Toon et al., 2000; Biele et al., 2001), for each instrument in a specific geophysical situation it is necessary to develop an appropriate classification scheme for PSCs. Lidars working at different wavelengths will measure different backscatter ratios $R_{||}$ and $R_{\perp}$. However, a classification of all known PSC types by lidar observation only is quite ambiguous. Other aerosols, for example smoke and soot from wildfires, can show the same scattering properties as PSCs (Siebert et al., 2000) and accompanying meteorological conditions have to be taken into account. Here we will concentrate on the three classical types of PSC, Ia, Ib, and II, as well as on an additional type which comprises all data which do not fit one of the three classical types. We call this additional type of PSC "mixed clouds".

Figure 3 shows all PSC measurements performed in both polarization directions in the form of a two-dimensional histogram. The axes are on logarithmic scales (the backscatter ratios in parallel and cross-polarization at a wavelength of 532 nm) and the colour code describes the number of data points which fit with one certain $R_{||}$, $R_{\perp}$ combination. The data used are those of all PSC observations taken from each altitude bin of 150 m width and with 1 h integration time. In addition solid black lines show values of constant aerosol depolarization δ_{Aer}. For the classification of PSC observations it is necessary to have values for both backscatter ratios.

We use the general results obtained previously by, for example, Browell et al. (1990) as a guideline and state that PSCs of type Ia must show high values of aerosol depolarization ($\delta_{\mathrm{Aer}} \gg \delta_{\mathrm{Mol}}$) but low values of $R_{||}$. PSCs of type Ib are liquid and thus show in principle no aerosol depolarization δ_{Aer} and a moderate backscatter ratio $R_{||}$. Type II PSCs are again solid and thus show a depolarization $\delta_{\mathrm{Aer}} \gg \delta_{\mathrm{Mol}}$. Due to the relatively large amount of water in the stratosphere (in comparison with nitric acid) both backscatter ratios can be quite large.

In Fig. 3 there are obviously three regions where PSC observations cluster. The first group is at low backscatter ratios in the parallel polarization channel having values $R_{||} \ll 2$, while the backscatter ratio in cross-polarization reaches quite large values up to $R_{\perp} \approx 30$. These data show large aerosol depolarizations of up to $\delta_{\mathrm{Aer}} \approx 30\%$ and can be associated with PSCs of type Ia, marked by the white ellipse.

The second group of PSC observations can be found at larger values of $R_{||}$, up to 5. However, the backscatter ratio in

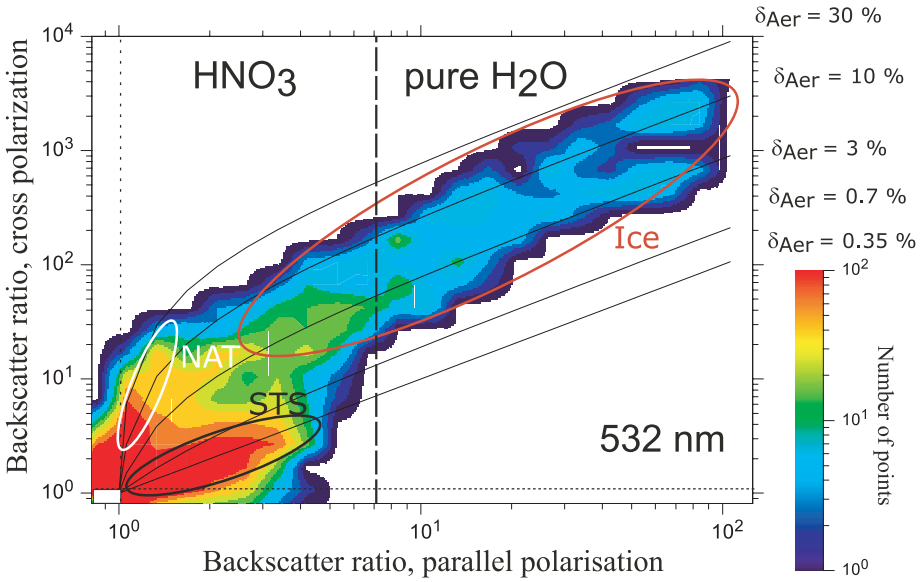

Fig 3. Two-dimensional histogram of number of PSC observations by the Bonn University lidar in both polarization directions (1997–2004). For details see text.

cross-polarization is very small ($R_\perp < 3$), resulting in small aerosol depolarization $\delta_{\mathrm{Aer}} < 0.7\%$. Clouds showing nearly no aerosol depolarization must be mostly liquid and thus these measurements are associated with PSCs of type Ib, shown by the black ellipse.

The third group of PSC observations exists at large values of both backscatter ratios. Due to the limited amount of HNO_3 in the stratosphere the observations at $R_{||} > 7$ must consist of water and are thus PSCs of type II. However, type II PSCs can also have smaller values of $R_{||}$. Overall they show an aerosol depolarization of $\delta_{\mathrm{Aer}} \approx 3$–$10\%$. The region of ice PSCs is marked by the red ellipse.

Finally, it is obvious that these classifications do not cover all PSC measurements. The remaining data points are assumed to be mixed clouds, containing a strong and weak depolarizing scatterer such as NAT or STS. A dominant constituent, however, cannot be determined. To avoid confusion between PSCs and the background aerosol, aerosol signatures are defined as PSCs if they are observable over an altitude range of 450 m or more and have a backscatter ratio in either of the two green channels (532 nm) which is larger than 1.06. While the amount of background aerosol was quite large ($R_{||} \approx 1.2$) in 1994–1995 (Müller et al., 1995) due to the eruption of Mount Pinatubo in 1991 this aerosol load has reduced to $R_{||} \approx 1.05$ since 1997 due to sedimentation. To also include PSCs of very small vertical extent (300 m or less) backscatter ratios in only one or two altitude bins are accepted as PSCs if the backscatter ratio in at least one channel is larger than 1.5. The classification scheme is summarized in Table 1.

This scheme can now be used to analyse each single PSC observation with regard to cloud type. Figure 4 gives an example

Table 1. Classification scheme for PSC observations with the Bonn University Lidar at Esrange at 532 nm wavelength

PSC type	Backscatter ratio, $R_{||}$	Aerosol depolarization, δ_{Aer}
Background aerosol	$R_{||} < 1.06$	
PSC Ia (NAT)	$1.06 < R_{||} < 2$	>10.0%
PSC Ib (STS)	$1.06 < R_{||} < 5$	<0.7%
PSC II (ice) either	$2 < R_{||} < 7$	>2.0%
or	$7 < R_{||}$	

of a PSC measurement on 12 December 2001. The observation started at 02:10 UT and lasted for 43 min. Altitude profiles of $R_{||}$ and $R_\perp$ as well as the classification of the individual PSC layers are shown. The PSC covers the altitude range from 21.3 to 25.8 km and contains all four PSC types, NAT, STS, ice and mixed clouds. This classification has been performed for all PSC measurements and Fig. 5 shows the absolute number of cases and their relative rates of occurrence. Altogether there were 8619 PSC measurements. The largest number of these data are classified as PSCs of type Ib (39%). Mixed clouds make up 37%, i.e. nearly the same number of observations. The remaining observations are PSC Ia (15%) and PSC II (9%). Thus all three classical PSC types are observed at Esrange; however, for a large number of the clouds the composition cannot be unambiguously determined.

The classification of the observed PSCs also gives the altitude distribution of the different cloud types. Most PSCs occur in the 18–28 km altitude range with a maximum occurrence rate at about 23–26 km altitude independent of the particular cloud

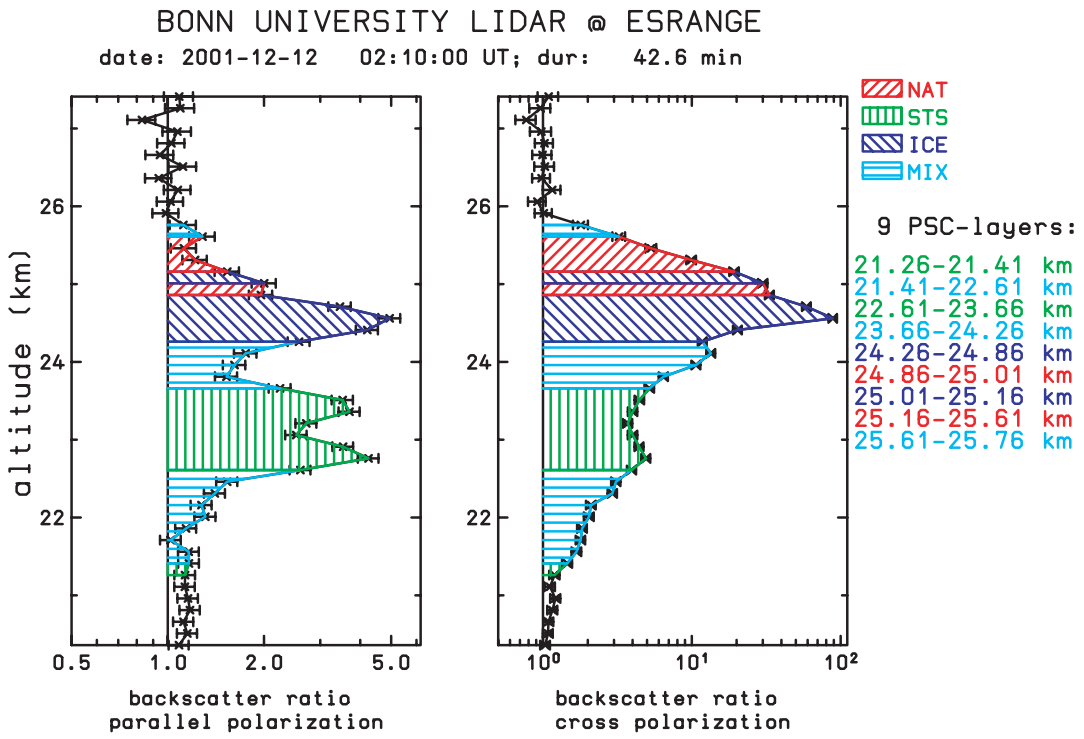

Fig 4. PSC measurement by the Bonn University lidar on 12 December 2001. The figures shows the backscatter ratios in the parallel (left) and cross-polarized (right) channels as well as a classification of the different PSC types.

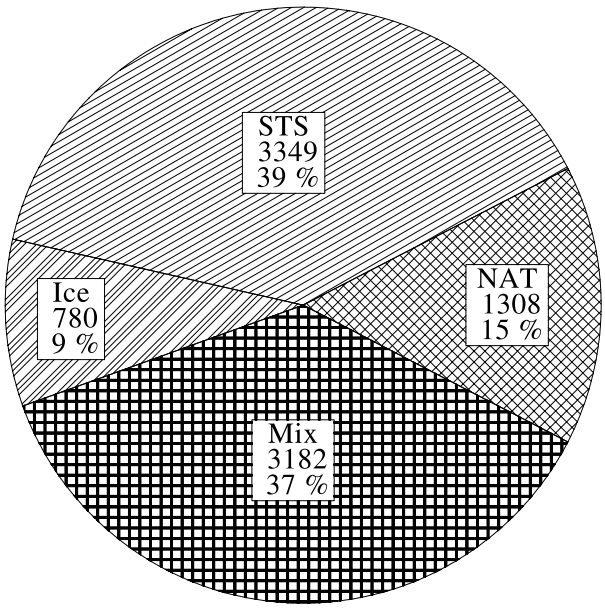

Fig 5. Classification of PSC measurements by the Bonn University lidar during the years 1997–2004.

type (see Fig. 6). The altitude distributions of the different cloud types reveal some differences, in particular the STS clouds show two peaks, one at about 23 km and a second at about 19 km. Although the coarse structure of the PSC altitude distribution is similar during the different years, details reveal differences which are attributed to different meteorological situations, i.e. different atmospheric temperature structures. In fact, most of the low-altitude cloud signatures, below 16 km altitude, are from measurements in December 2003.

5. Conditions of occurrence of PSCs

The atmospheric temperature must fall below a certain threshold for PSCs to come into existence. The classification of the cloud type in each individual altitude bin allows a determination of the maximum atmospheric temperature which existed in a given altitude range. The ECMWF T106 analysis provides temperature profiles on a synoptic-scale grid. The results of a comparison of the necessary temperatures for existence of PSCs and the synoptic-scale temperatures are shown in Fig. 7. The relative frequency of PSC observations which are explainable by the ECMWF T106 temperatures is shown.

More than 80% of the NAT clouds can be explained by the synoptic-scale temperatures. For STS and mixed PSCs this is the case for only about 35% each and for ice PSCs it is only 3.5%. This simple comparison does not depend on the details of the mechanism of particle formation or the value of the formation temperature, which falls below the existence or condensation temperature (e.g. Carslaw et al., 1998a; Luo et al., 2003; Drdla and Browell, 2004). Using the existence temperatures for NAT, STS and ice clouds, the comparison shows unambiguously that

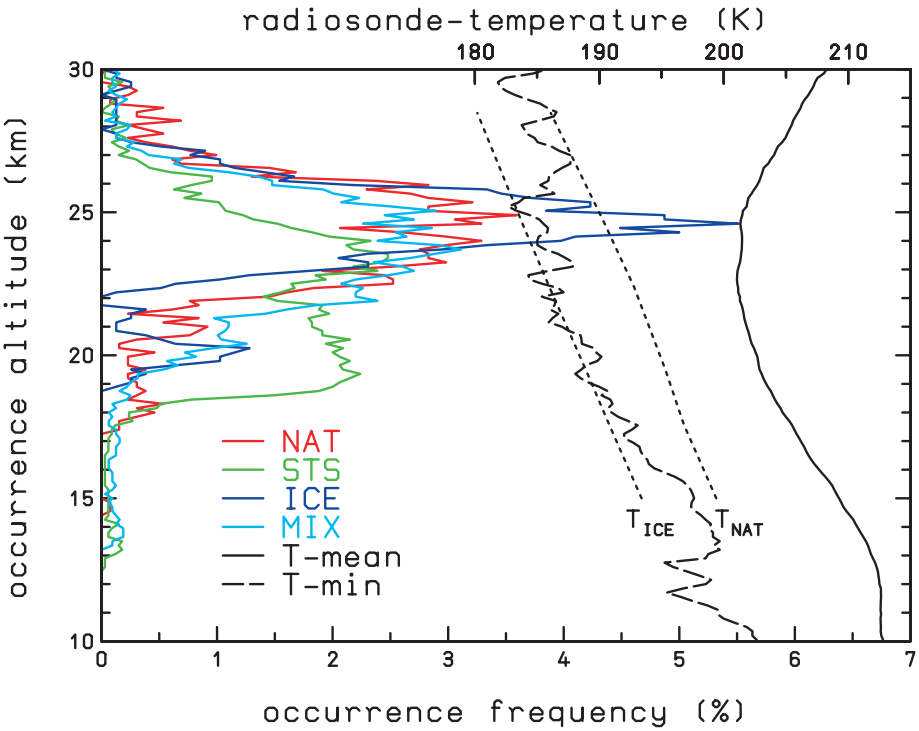

Fig 6. Altitude of PSC occurrence for each PSC type, mean temperature profile and minimum temperature values near Esrange. The lower abscissa gives the relative occurrence frequency of the PSCs, the upper abscissa the temperature. The mean temperature profile is derived from more than 300 radiosondes, launched at Esrange during the months December to February from 1996 to 2004. The T-min profile shows for each altitude the observed minimum temperature from different radiosonde flights.

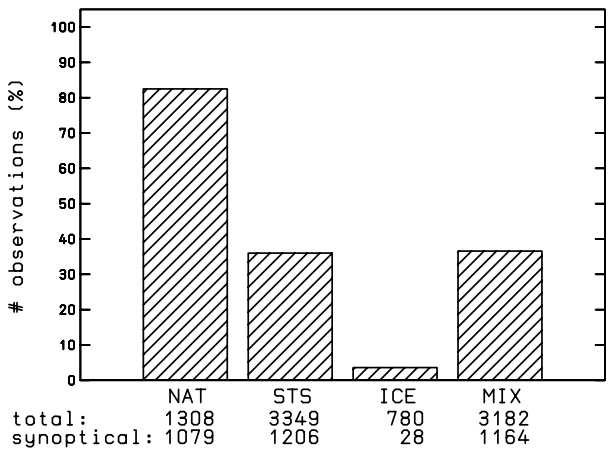

Fig 7. Relative and absolute frequency of different PSC types which are explainable by the synoptic-scale ECMWF T106 temperatures.

the synoptic-scale temperatures do not allow the existence of most of the observed PSCs. To test the sensitivity of our results to temperature we have arbitrarily reduced the existence temperature of STS by 1 K. This reduces the fraction of STS which are explainable by synoptic temperatures by about 10% (from 35% to 25%) which confirms the conclusions of this analysis.

The peak in the PSC altitude distribution at about 24 km (Fig. 6) corresponds to the wide minimum in the mean temperature profile, reaching from about 23 to 25 km in altitude, derived from more than 300 radiosondes launched at Esrange in the months December to February during 1997–2004. At an altitude of 25 km data from about 220 radiosondes are available and at 30 km there are data from about 150 radiosondes. In addition to the mean temperature profile the overall minimum temperature at each altitude measured by the radiosondes is shown. These coldest temperatures allow the existence of NAT particles throughout most of the regions of occurrence of PSCs; however, ice cloud formation is hardly supported by these temperatures. Orographically induced gravity waves regularly lead to spatial and temporal modulation of the stratospheric temperature profile and thus allow the existence of PSCs in the wave temperature minima. The propagation conditions for stationary gravity waves can be estimated using critical level filtering. For the PSC events which were not explainable by the synoptic-scale temperatures an analysis of the propagation conditions of orographically induced gravity waves was conducted. Figure 8 shows the relative number of PSC observations during which the lower atmosphere was transparent up to the middle stratosphere for orographically induced gravity waves. Also given are the absolute numbers of PSC observations when wave cooling was

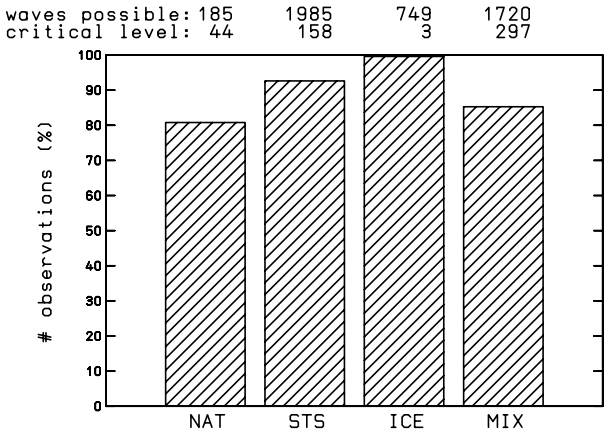

Fig 8. Relative and absolute frequency of PSC observations during which gravity wave propagation was possible and large-scale (synoptic) temperatures are above the existence temperature. At the top of the figure the absolute numbers of measurements are given where wave cooling was possible and when critical level filtering occurred for non-synoptic PSCs.

possible and when critical level filtering occurred in an altitude below the PSC layer. This analysis is performed only for those data that are not explainable by the synoptic-scale temperatures.

For about 80% of these NAT events the atmosphere was transparent for orographically induced gravity waves. The corresponding numbers are 93% for STS clouds, 99% for ice PSCs and 85% for mixed clouds. The analysis of the ground wind reveals that the horizontal wind speed was greater than 10 m s^{-1} in 66% of all cases. A wind speed of 10 m s^{-1} is large enough for major gravity wave excitation (Dörnbrack and Leutbecher, 2001). Only 97 cases out of 4639 showed velocities below 5 m s^{-1}. The majority of all PSC observations above Esrange can be attributed to orographically induced gravity waves.

Our results are quite different from those of other long-term PSC observations by lidar. PSC observations at Thule, Greenland (77°N, 69°W; di Sarra et al., 2002) show no ice clouds, very varying amounts of NAT cloud (between 8.4 and 55.4% in different years) and only very small amounts of STS cloud (5.3–7.8%). Although the classification schemes are quite different (PSCs are identified as Ib for $R \geq 1.5$ and $\delta < 10\%$ by di Sarra et al., 2002) the influence of gravity waves on polar stratospheric clouds is much less than at Esrange, as can be seen from the missing ice cloud observations. This is particularly remarkable because the Thule measurements were performed during 1990–1997, comprising several cold winters with a stable vortex. During these winters synoptic ice PSCs would have been expected. A similar situation is given at the Arctic station of Ny-Ålesund (79°N, 12°E; Müller et al., 2004). Since 1995 there have been lidar observations each winter; however, no ice PSCs have been observed. On 75% of all days with PSC observations NAT clouds were observed and on 85% STS clouds. In particular simultaneous observations of solid and liquid particles in so-called sandwich structures occur regularly. Unlike Esrange, Ny-Ålesund is located near the centre of the polar vortex and thus shows synoptic PSCs. The McMurdo station in Antarctica (78°S, 167°E) is located inside the southern polar vortex, which is much more stable than the Arctic polar vortex and which allows continuous evolution of PSCs. Here NAT clouds occur on almost every day when PSCs are observed (96%; Müller et al., 2004). STS clouds occur more seldom (13%) and ice clouds are seen on fewer than 9% of all days when PSCs occur. This rate of occurrence of ice clouds at McMurdo is comparable to the frequency of observation of type II PSCs at Esrange. At the edge of the southern polar vortex (Dumont d'Urville; 66°S, 140°E) the PSC situation is even more different, as can be seen from Santacesaria et al. (2001). The occurrence of the different types and the PSC altitude depends on the season. At the beginning of the winter only type Ia and Ib are observed; type II occurs exclusively during a certain time in mid-winter. Furthermore a decrease in PSC altitude is observed during the winter. These effects can be attributed to a stable polar vortex and variations of the vortex during the season. In the Northern Hemisphere, in particular at Esrange, the existence of PSCs is mostly determined by gravity wave activity in the atmosphere; there is therefore neither a seasonally dependent occurrence of individual PSC types nor a decrease of PSC altitude during the winter.

6. Summary

Polar stratospheric clouds have been observed with the Bonn University lidar at Esrange since 1997 during more than 15% of the measurement time. A classification of the observed PSCs is possible for all data and reveals four different cloud types which show very different rates of occurrence. While STS and mixed clouds occur frequently (more than three-quarters of all PSC observations), NAT and ice PSCs seldom occur. The relative rate of occurrence of ice PSCs is only 9%. A comparison of the necessary existence temperatures with the synoptic-scale temperatures provided by ECMWF T106 analyses reveals that most of the STS, ice and mixed PSCs could not exist in the synoptic-scale temperature field. However, the analysis of the propagation conditions for orographically induced gravity waves shows that the atmosphere was transparent for gravity waves for more than 80% of all non-synoptic PSC observations. Thus the existence of polar stratospheric clouds above Esrange is dominated by orographically induced gravity waves, a situation which is different from the observations at Thule, Ny-Ålesund, McMurdo and Dumont d'Urville.

7. Acknowledgments

We thank the staff of Esrange for their ever quick and uncomplicated support during the measurement campaigns. The measurements were funded by the German and European ozone research programmes and by a Envisat Validation project grant from the DLR Erdbeobachtung FKZ 50 EE 0009. Finally we thank NILU for providing the ECMWF T106 data.

References

Biele, J., Beyerle, G. and Baumgarten, G. 2000. Polarization lidar: corrections of instrumental effects. *Opt. Express* **7**, 427–435.

Biele, J., Tsias, A., Luo, B. P., Carslaw, K. S., Neuber, R. and co-authors 2001. Nonequilibrium coexistence of solid and liquid particles in Arctic stratospheric clouds. *J. Geophys. Res.* **106**, 22 991–23 007.

Blum, U. 2003. *Lidarbeobachtungen der Polaren Atmosphäre: Wolken und Wellen—Phänomene und Mechanismen*. PhD Thesis BONN-IR-2003–11. Universität Bonn, Bonn.

Blum, U. and Fricke, K. H. 2005. The Bonn University Lidar at the Esrange: technical description and capabilities for atmospheric research. *Ann. Geophys.* **23**, 1645–1658.

Blum, U., Fricke, K. H., Baumgarten, G. and Schöch, A. 2004. Simultaneous lidar observations of temperatures and waves in the polar middle atmosphere on the east and west side of the Scandinavian mountains: a case study on 19/20 January 2003. *Atmos. Chem. Phys.* **4**, 809–816.

Browell, E. V., Butler, C. F., Ismail, S., Robinette, P. A., Carter, A. F. and co-authors 1990. Airborne lidar observations in the wintertime Arctic stratosphere: polar stratospheric clouds. *Geophys. Res. Lett.* **17**, 385–388.

Carslaw, K. S., Kettleborough, J. A., Northway, M. J., Davies, S., Gao, R.-S. and co-authors 2002. A vortex-scale simulation of the growth and sedimentation of large nitric acid hydrate particles. *J. Geophys. Res.* **107**, doi:10.1029/2001JD000467.

Carslaw, K. S., Wirth, M., Tsias, A., Luo, B. P., Dörnbrack, A. and co-authors 1998a. Particle microphysics and chemistry in remotely observed mountain polar stratospheric clouds. *J. Geophys. Res.* **103**, 5785–5796.

Carslaw, K. S., Wirth, M., Tsias, A., Luo, B. P., Dörnbrack, A. and co-authors 1998b. Increased stratospheric ozone depletion due to mountain-induced atmospheric waves. *Nature* **391**, 675–678.

Crutzen, P. and Arnold, F. 1986. Nitric acid cloud formation in the cold Antarctic stratosphere: a major cause for springtime 'ozone hole'. *Nature* **324**, 651–655.

Deshler, T., Larsen, N., Weissner, C., Schreiner, J., Mauersberger, K. and co-authors 2003. Large nitric acid particles at the top of an Arctic stratospheric cloud. *J. Geophys. Res.* **108**, doi:10.1029/2003JD003479.

di Sarra, A., Cacciani, M., Fiocco, G., Fuà, D. and Jørgensen, T. S. 2002. Lidar observations of polar stratospheric clouds over northern Greenland in the period 1990–1997. *J. Geophys. Res.* **107**, doi:10.1029/2001JD001074.

Dörnbrack, A., Birner, T., Fix, A., Flentje, H., Meister, A. and co-authors 2002. Evidence for inertia gravity waves forming polar stratospheric clouds over Scandinavia. *J. Geophys. Res.* **107**, doi:10.1029/2001JD000452.

Dörnbrack, A. and Leutbecher, M. 2001. Relevance of mountain waves for the formation of polar stratospheric clouds over Scandinavia: a 20 year climatology. *J. Geophys. Res.* **106**, 1583–1593.

Drdla, K. and Browell, E. V. 2004. Microphysical modelling of the 1999–2000 arctic winter: 3. Impact of homogeneous freezing on polar stratospheric clouds. *J. Geophys. Res.* **109**, doi:10.1029/2003JD0004352.

Fahey, D. W., Gao, F. S., Carslow, K. S., Kletteborough, J., Popp, P. J. and co-authors 2001. The detection of large HNO_3-containing particles in the winter arctic stratosphere. *Science* **291**, 1026–1031.

Fritts, D. C., 1984. Gravity wave saturation in the middle atmosphere: a review of theory and observations. *Rev. Geophys.* **22**(3), 275–308.

Fromm, M., Alfred, J. and Pitts, M. 2003. A unified. long-term, high-latitude stratospheric aerosol and cloud database using SAM II, SAGE II, and POAM II/III data: algorithm description, database definition, and climatology. *J. Geophys. Res.* **108**, 4366, doi:10.1029/2002JD002772.

Gille, J. C., Bailey, P. L. and Craig, C. A. 1996. Revised reference model for nitric acid. *Adv. Space Res.* **18**(9/10), 125–138.

Hanson, D. and Mauersberger, K. 1988. Laboratory studies of the nitric acid trihydrate: implications for the south polar stratosphere. *Geophys. Res. Lett.* **15**, 855–858.

Höpfner, M., Stiller, G., von Claremann, T., Fischer, H., Luo, B. and co-authors 2005. Evidence for β-NAT in MIPAS mid-infrared limb emission spectra of PSCs by new refractive index data. *Geophys. Res. Abstr.* **7**, 08 395.

Labitzke, K. and Naujokat, B. 2000. The lower Arctic stratosphere in winter since 1952. *SPARC Newsletter* **15**, 11–14.

Labitzke, K., Naujokat, B. and Kunze, M. 2005. The lower Arctic stratosphere in winter since 1952: an update. *SPARC Newsletter* **24**, 27–28.

Luo, B. P., Voigt, C., Flueglistaler, S. and Peter, T. 2003. Extreme NAT supersaturation in mountain wave ice PSCs: a clue to NAT formation. *J. Geophys. Res.* **108**, doi:10.1029/2002JD003104.

MacKenzie, A. R. 1995. On the theories of type 1 polar stratospheric cloud formation. *J. Geophys. Res.* **100**, 11 275–11 288.

McCormick, M. P., Steel, H. M., Hamill, P., Chu, W. P. and Swissler, T. J. 1982. Polar stratospheric cloud sightings by SAM II. *J. Atmos. Sci.* **39**, 1387–1397.

Müller, K.-P., Langer, M., Römke, K. and Fricke, K. H. 1995. *PSCs and Aerosol Above Andøya during Sesame Winters 1993/94 and 1994/95. Air Pollution Report 56*. European Commission, Luxembourg, 122–125.

Müller, M., Neuber, R., Massoli, P., Cairo, F., Adriani, A. and co-authors 2004. Differences in Arctic and Antarctic PSC occurrence as observed by lidar in Ny-Ålesund (79°N, 12°E) and McMurdo (78°S, 167°E). *Atmos. Chem. Phys. Discuss.* **4**, 6837–6866.

Murray, F. W. 1967. On the computation of saturation vapor pressure. *J. Appl. Meteorol.* **6**, 203–204.

Naujokat, B. and Grunow, K. 2003. The stratospheric Arctic winter 2002/03: balloon flight planning by trajectory calculations. *Proceedings of the 16th ESA Symposium on European Rocket and Balloon Programmes and Related Research, St Gallen, Switzerland, 2003*, ESA-SP-530, ESA Publication Division, Noordwijk, The Netherlands, 421–425.

Naujokat, B., Krüger, K., Matthes, K., Hoffmann, J., Kunze, M. and co-author 2002. The early major warming in December 2001—exceptional? *Geophys. Res. Lett.* **29**, 2023, doi:10.1029/2002GL015316.

Peter, T. 1997. Microphysics and heterogeneous chemistry of polar stratospheric clouds. *Ann. Rev. Phys. Chem.* **48**, 785–822.

Pool, L. R. and McCormick, M. P. 1988. Airborne lidar observations of Arctic polar stratospheric clouds: indications of two distinct growth stages. *Geophys. Res. Lett.* **15**, 21–23.

Pool, L. R. and Pitts, M. C. 1994. Polar stratospheric cloud climatology based on Stratospheric Aerosol Measurements II observations from 1978 to 1989. *J. Geophys. Res.* **99**, 13 083–13 089.

Santacesaria, V., MacKenzie, A. R. and Stefanutti, L. 2001. A climatological study of polar stratospheric clouds (1989–1997) from lidar measurements over Dumont d'Urville (Antarctica). *Tellus* **53B**, 306–321.

Siebert, J., Timmis, C., Vaughan, G. and Fricke, K. H. 2000. A strange cloud in the Arctic summer stratosphere 1998 above Esrange (68°N), Sweden. *Ann. Geophys.* **18**, 505–509.

Solomon, S. 1999. Stratospheric ozone depletion: a review of concepts and history. *Rev. Geophys.* **37**, 275–316.

Spang, R., Riese, M. and Offermann, D. 2001. CRISTA-2 observations of the south polar vortex in winter 1997: a new dataset for polar process studies. *Geophys. Res. Lett.* **28**, 3159–3162.

Steel, H. M., Hamill, P., McCormick, M. P. and Swissler, T. J. 1983. The formation of polar stratospheric clouds. *J. Atmos. Sci.* **40**, 2055–2067.

Stein, B., Wedekind, C., Wille, H., Immler, F., Müller, M. and co-authors 1999. Optical classification, existence temperatures, and coexistence of different polar stratospheric cloud types. *J. Geophys. Res.* **104**, 23 983–23 993.

Størmer, C., 1929. Remarkable clouds at high altitudes. *Nature* **123**, 260–261.

Tabazadeh, A. and Toon, O. B. 1996. The presence of metastable HNO_3/H_2O solid phase in the stratosphere inferred from ER 2 data. *J. Geophys. Res.* **101**, 9071–9078.

Toon, O. B., Hamill, P., Turco, R. P. and Pinto, J. 1986. Condensation of HNO_3 and HCl in the winter polar stratospheres. *Geophys. Res. Lett.* **13**, 1284–1287.

Toon, O. B., Tabazadeh, A., Browell, E. V. and Jordan, J. 2000. Analysis of lidar observations of Arctic polar stratospheric clouds during January 1989. *J. Geophys. Res.* **105**, 20 589–20 615.

Toon, O. B. and Tolbert, M. A. 1995. Spectroscopic evidence against nitric acid trihydrate in polar stratospheric clouds. *Nature* **375**, 218–221.

Tsias, A., Wirth, M., Carslaw, K. S., Biele, J., Mehrtens, H. and co-authors 1999. Aircraft lidar observations of an enhanced type Ia polar stratospheric clouds during APE-POLECAT. *J. Geophys. Res.* **104**, 23 961–23 969.

Voigt, C., Schreiner, J., Kohlmann, A., Zink, P., Mauersberger, K. and co-authors 2000. Nitric acid trihydrate (NAT) in polar stratospheric clouds. *Science* **290**, 1756–1758.

Volkert, H. and Intes, D. 1992. Orographically forced stratospheric waves over northern Scandinavia. *Geophys. Res. Lett.* **19**, 1205–1208.

Young, A. T., 1980. Revised depolarization corrections for atmospheric extinction. *Appl. Optics* **19**, 3427–3428.